Volume 52
Number 13
7 April 2023
Pages 3909-4262

Dalton Transactions

An international journal of inorganic chemistry

rsc.li/dalton

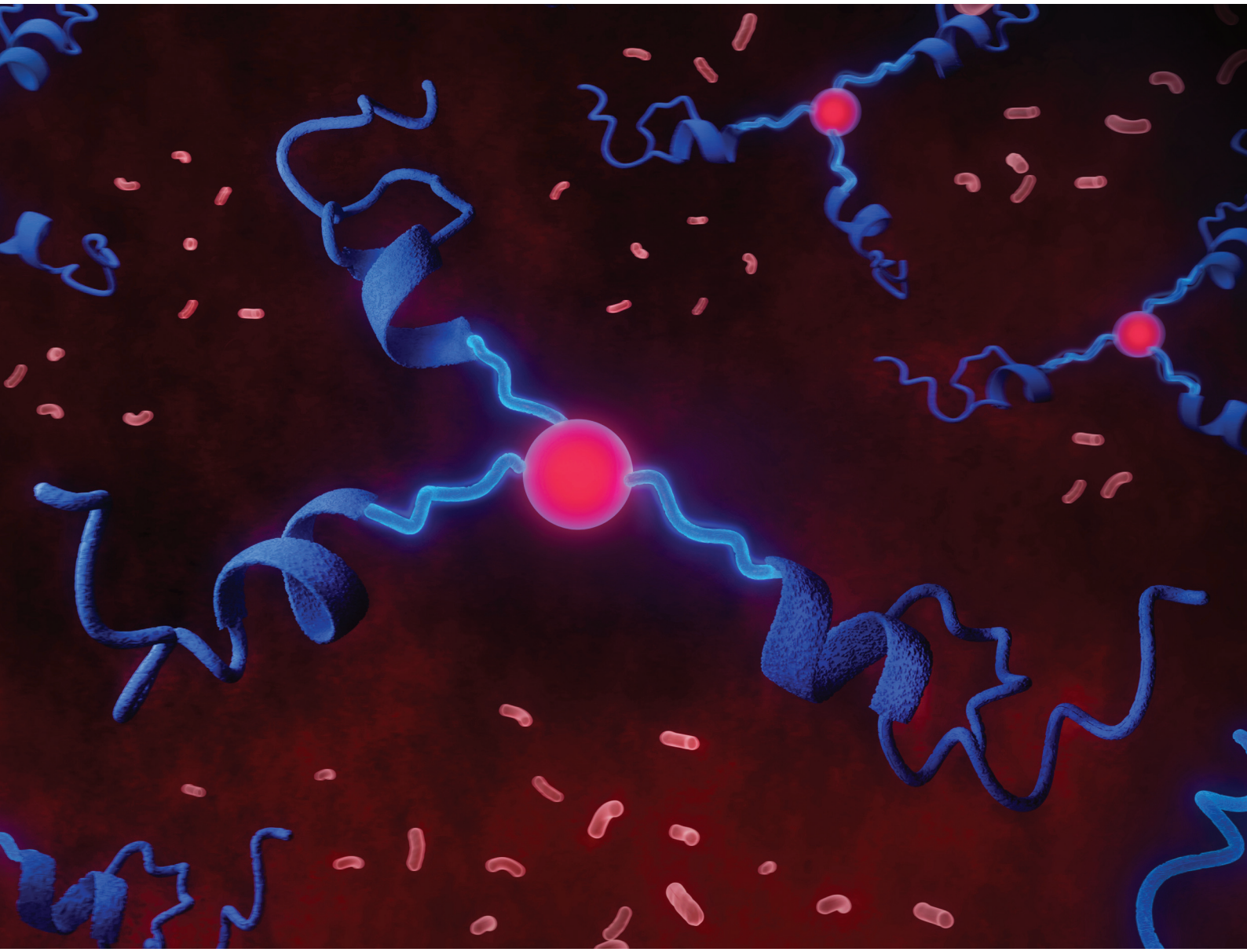

ISSN 1477-9226

ROYAL SOCIETY OF CHEMISTRY

PAPER

Stefania Galdiero, Annarita Falanga *et al.*
Synthesis of temporin L hydroxamate-based peptides and evaluation of their coordination properties with iron(III)

Dalton Transactions

ROYAL SOCIETY OF CHEMISTRY

PAPER

View Article Online
View Journal | View Issue

Cite this: *Dalton Trans.*, 2023, **52**, 3954

Synthesis of temporin L hydroxamate-based peptides and evaluation of their coordination properties with iron(III)†

Rosa Bellavita, [a] Linda Leone, [b] Angela Maione,[c] Lucia Falcigno,[a] Gabriella D'Auria,[a] Francesco Merlino, [a] Paolo Grieco,[a] Flavia Nastri, [b] Emilia Galdiero,[c] Angela Lombardi, [b] Stefania Galdiero *[a] and Annarita Falanga *[d]

Received 22nd December 2022,
Accepted 24th January 2023

DOI: 10.1039/d2dt04099a

rsc.li/dalton

Ferric iron is an essential nutrient for bacterial growth. Pathogenic bacteria synthesize iron-chelating entities known as siderophores to sequestrate ferric iron from host organisms in order to colonize and replicate. The development of antimicrobial peptides (AMPs) conjugated to iron chelators represents a promising strategy for reducing the iron availability, inducing bacterial death, and enhancing simultaneously the efficacy of AMPs. Here we designed, synthesized, and characterized three hydroxamate-based peptides **Pep-cyc1**, **Pep-cyc2**, and **Pep-cyc3**, derived from a cyclic temporin L peptide (**Pep-cyc**) developed previously by some of us. The Fe^{3+} complex formation of each ligand was characterized by UV-visible spectroscopy, mass spectrometry, and IR and NMR spectroscopies. In addition, the effect of Fe^{3+} on the stabilization of the α-helix conformation of hydroxamate-based peptides and the cotton effect were examined by CD spectroscopy. Moreover, the antimicrobial results obtained *in vitro* on some Gram-negative strains (*K. pneumoniae* and *E. coli*) showed the ability of each peptide to chelate efficaciously Fe^{3+} obtaining a reduction of MIC values in comparison to their parent peptide **Pep-cyc**. Our results demonstrated that siderophore conjugation could increase the efficacy and selectivity of AMPs used for the treatment of infectious diseases caused by Gram-negative pathogens.

Introduction

Iron is a vital metabolic cofactor for both humans and bacteria that compete for metal acquisition.[1,2] Iron has a complex and multifaceted biological role in humans.[3] When present at high concentrations,[4] it might be toxic causing oxidative stress; thus, its bioavailability is strictly controlled by iron-binding proteins.[5] Interestingly, iron scavenging is also key to limiting iron access to invading microorganisms, which also require iron to function properly. Generally, prokaryotes require *ca.* 10^{-6} M of iron to colonize and replicate, but the poor solubility of the metal at neutral pH limits its concentration to 10^{-18} M.[6] As a matter of fact, bacteria use different strategies to acquire iron from the host environments. Among these, one strategy is the synthesis and secretion of small molecules known as siderophores,[7,8] which acquire iron from tissues, fluids, and cells and translocate iron–siderophore complexes inside cells by exploiting porins, which are located in the bacterial outer membranes.[9,10]

The large structural and functional diversity of siderophores secreted by bacteria inspired the design of new antimicrobial molecules able to capture iron with higher affinity, influencing iron acquisition, transport, and storage that are essential for bacterial survival.[11,12] In particular, siderophores are commonly classified into catecholate, hydroxamate, carboxylate, and phenolate according to the moieties involved in iron chelation.[13–15] Ferric iron (Fe^{3+}) is coordinated by six donor atoms in an octahedral structure; further these ligands can be classified according to whether they have two (bidentate), three (tridentate), or six (hexadentate) donor atoms available for coordination to Fe^{3+}.[16] Hexadentate complexes present the greatest stability; in fact, most siderophores produced by microorganisms use hexadentate ligands.[17,18]

Given the different roles of siderophores in both the physiology and pathogenicity of bacteria, exploiting or targeting them represents a challenging strategy for the development of

[a]*Department of Pharmacy, University of Naples "Federico II", Via Domenico Montesano 49, 80138 Naples, Italy. E-mail: stefania.galdiero@unina.it*
[b]*Department of Chemical Sciences, University of Napoli "Federico II", Napoli, Italy*
[c]*Department of Biology, University of Naples Federico II, Via Cinthia, 80126 Naples, Italy*
[d]*Department of Agricultural Sciences, University of Naples "Federico II", via Università 100, 80055 Portici, Italy. E-mail: annarita.falanga@unina.it*
† Electronic supplementary information (ESI) available. See DOI: https://doi.org/10.1039/d2dt04099a

new antimicrobial molecules.[19] Generally, siderophores are conjugated to currently used antibiotics to enhance their activity since siderophore–antibiotic conjugates can exploit the iron uptake pathways to transport the antibiotic into the bacterial cell, which then acts on its intracellular target.[20] This strategy is known as the Trojan horse approach.[21] Similarly, antimicrobial peptides (AMPs), which are widely studied and considered a promising alternative to traditional antibiotics for their mode of action,[22–28] may be linked to siderophore–iron chelators to reduce the iron availability for bacterial growth and enhance their efficacy (Fig. 1).[29–32]

In this work, we introduced the hydroxamate moiety as a coordinating functional group into a cyclic AMP that was recently developed by some of us.[33] This synthetic cyclic AMP, hereafter named **Pep-cyc**, belongs to temporins, which is one of the most abundant AMP families in nature.[34,35] Among the different temporin isoforms, our research has been focused on the temporin L (TL) isoform, with the aim to introduce modifications that may lead to an improved therapeutic index as it is highly hemolytic in its native form.[36–39] **Pep-cyc** (FVPWF [KKF*l*E]RIL) is derived from a detailed structure–activity relationship (SAR) campaign conducted on the analogue [Pro^3, DLeu^9]TL, in which the α-helix conformation was stabilized through the application of different *i*,*i* + 4 intramolecular macrocyclization strategies.[33] In particular, **Pep-cyc** was obtained by the introduction of a lactam bridge between positions 6 and 10 and was identified as the most promising antimicrobial candidate due to its potent activity against Gram-positive strains and some *Candida* species, with the minimal inhibitory concentration (MIC) ranging from 3.12 μM to 12.5 μM.[40] Furthermore, it showed activity against *A. baumannii* (MIC of 3.12 μM), a Gram-negative strain.[33] Herein, to improve the antimicrobial efficacy of **Pep-cyc** against Gram-negative superbugs, such as *E. coli* and *K. pneumoniae*, a hydroxamate chelating moiety was covalently bound through linkers of different lengths at its C-terminal helical region, resulting in being able to chelate and subtract iron from the bacteria and consequently reduce its growth. We reported the synthesis of three cyclic peptides **Pep-cyc1**, **Pep-cyc2**, and **Pep-cyc3** containing hydroxamate chelating units anchored to their C-terminus as pendants. The Fe^{3+} complex formation was studied by UV-visible spectroscopy, mass spectrometry, and infrared (IR) and NMR spectroscopies. The effect of Fe^{3+} on the α-helix conformation of hydroxamate-based peptides was investigated by circular dichroism (CD); the Cotton effect in the near visible region induced by the interaction of peptides with Fe^{3+} was evaluated. In addition, the ability of hydroxamate-based peptides to chelate iron was assessed *in vitro* on some Gram-negative strains using iron-supplemented Mueller–Hinton broth. We found significant agreement between the antibacterial and iron coordination studies, which point to these peptides as effective Fe^{3+} chelators and new-generation antimicrobial molecules.

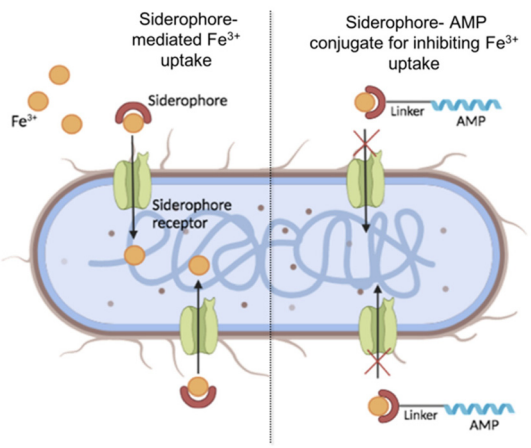

Fig. 1 Schematic representation of Fe^{3+} uptake by natural siderophores (on the left) and its hypothetical inhibition by the siderophore–AMP conjugate.

Experimental

Materials

N^{α}-Fmoc-protected conventional amino acids were purchased from GL Biochem Ltd (Shanghai, China). Unnatural amino acids such as Fmoc-L-Lys(Alloc)-OH and Fmoc-L-Glu(OAll)-OH, [2-[2-(Fmoc-amino)ethoxy]ethoxy]acetic acid (Fmoc-PEG2-OH), *N*,*N*-diisopropylethylamine (DIEA), piperidine, trifluoroacetic acid (TFA), (7-azabenzotriazol-1-yloxy)tripyrrolidinophosphonium hexafluorophosphate (PyAOP), and the resin 2-chlorotrityl-*N*-Fmoc-hydroxylamine were acquired from Iris-Biotech GMBH. Coupling reagents such as *N*,*N*,*N*′,*N*′-tetramethyl-*O*-(1*H*-benzotriazol-1-yl) uranium hexafluorophosphate (HBTU), 1-hydroxybenzotriazole (HOBt), (1-[bis(dimethylamino)methylene]-1*H*-1,2,3-triazolo[4,5-*b*] pyridinium 3-oxide hexafluorophosphate) (HATU), and 1-hydroxy-7-azabenzotriazole (HOAt) were commercially obtained from GL Biochem Ltd (Shanghai, China).

6-(Fmoc-amino)hexanoic acid (Fmoc-6-Ahx)-OH, L-2-(Fmoc-amino)butyric acid (Fmoc-GABA-OH), 1,3-dimethylbarbituric acid, tetrakis(triphenylphosphine)palladium(0) [$Pd(PPh_3)_4$], and iron(III) chloride ($FeCl_3$) were purchased from Sigma-Aldrich/Merck.

Methods

Hydroxamate-based cyclic peptide synthesis. Hydroxamate-based peptides were synthesized stepwise using solid-phase peptide synthesis assisted by ultrasound irradiation.[33] 2-Chlorotrityl-*N*-Fmoc-hydroxylamine polymer was used as a resin to yield hydroxamic acid moiety in C-terminus.[41] The resin was conditioned with dimethylformamide (DMF) for 30 minutes and then the Fmoc group removal from hydroxylamine was performed using a solution of 20% piperidine in DMF solution (2 × 5 min) under gentle stirring at room temperature (rt). The coupling of the first reagent (Fmoc-Ahx-OH in **Pep-cyc1** and **Pep-cyc2**, or Fmoc-PEG2-OH in **Pep-cyc3**, 3 equiv.) was achieved in the presence of coupling reagents such

as HATU (3 equiv.), HOAt (3 equiv.), and DIPEA (6 equiv.) at room temperature (rt) for 12 h.[42] Then, the Fmoc group was removed by using 20% piperidine in DMF (2 × 5 min, under ultrasound irradiations), and then the assembly of the linear sequence was carried out through repeated cycles of Fmoc deprotection and coupling reactions. Each coupling reaction was performed using Fmoc-amino acid (3 equiv.), HBTU (3 equiv.), HOBt (3 equiv.) and DIPEA (6 equiv.) for 15 min under ultrasonic irradiation. For the formation of the lactam bridge, we employed allyl-protected lysine and glutamic acid [Lys-(Alloc)/Glu(OAll)] at positions 6 and 10 during the elongation of the peptide sequence.

After the complete synthesis of the linear sequence, the resin was washed with dichloromethane (DCM), dried and the side-chain-to-side-chain lactamization was performed. Firstly, the allyl deprotection was performed on a resin using a solution of $Pd(PPh_3)_4$ (0.15 equiv.) and 1,3-dimethylbarbituric acid (3 equiv.) as an allyl scavenger in dry DCM/DMF (3 : 2 v/v), and gently shaken for 1 h under argon.[42] Then, the resin was washed with DMF and DCM, and the allyl deprotection was repeated for a second time. After these two allyl-deprotection steps, the resin was washed with 0.5% sodium *N*,*N*-diethyldithiocarbamate solution in DMF (30 min × 2) and the complete removal of the allyl groups was checked by LC-MS analysis. Then, the lactamization between the free amine and carboxylic groups was coupled using PyAOP (3 equiv.), HOAt (3 equiv.), and DIEA (6 equiv.) dissolved in DMF, for 12 h at rt. After washing the resin with DMF and DCM, this conversion in the cyclic product was ascertained by LC-MS.

Finally, the peptides were released from the resin and the protecting groups were removed through treatment with the cleavage cocktail of TFA/TIS/H_2O (95 : 2.5 : 2.5, v/v/v) for 3 h at rt. Then, the resin was removed by filtration and the crude peptides were precipitated using cold diethyl ether by centrifuging at 6000 rpm for 15 min × 2. Finally, the crude peptides were dissolved in 10% acetonitrile (MeCN 0.1% TFA) in H_2O (0.1% TFA) and purified by reversed-phase high-pressure liquid chromatography (RP-HPLC) using a gradient of MeCN (0.1% TFA) in H_2O (0.1% TFA) from 10 to 90% over 20 min. All peptides were characterized for purity by analytical RP-HPLC and the correct molecular mass was confirmed through high-resolution mass spectrometry (HRMS) (see ESI, Fig. S1–S3†).

Spectrophotometric investigation of Fe^{3+} complexes. Spectrophotometric measurements were performed using a UV-Jasco V-750 using 0.1 cm quartz cells and $FeCl_3$ as the iron source. The UV-vis spectrum of each peptide at a concentration of 300 μM in MeOH was recorded prior to titration experiments. Before the titration, a small excess (1.1 eq.) of a mild base (DIPEA) was added to ensure full deprotonation of ligands. Each peptide placed in the cuvette was titrated with various volumes of a fresh solution of $FeCl_3$ solution in MeOH to achieve Fe^{3+} and peptide ratios between 0 and 0.8.[43] Each UV-vis spectrum was recorded in a wavelength ranging from 280 to 700 nm. During the titration, upon the addition of ferric iron to peptides, the solutions changed from colorless to red/pink.

The absorbance at 580 nm, attributed to the Fe^{3+}–hydroxamate complex, was used to calculate the fraction of the bound peptide at each point of the titration:

$$\alpha = \frac{A_{max} - A}{A_{max} - A_{min}}$$

where A is the value of absorbance at 580 nm at each point and A_{max} and A_{min} are the maximum and minimum values of absorbance at 580 nm found during the titration, corresponding to completely bound and free peptides, respectively. α was reported as a function of $[Fe^{3+}]$ and the linear regression method was applied to evaluate the stoichiometry of the Fe^{3+} complexes separately for each complex. The data points corresponding to low iron concentrations ($[Fe^{3+}]$ <30 μM for **Pep-cyc2** and **Pep-cyc3**; $[Fe^{3+}]$ <90 μM for **Pep-cyc1**) were not included in the linear regression analysis.

Data points were fit using the Hill equation

$$\alpha = \frac{[Fe^{3+}]^n}{[Fe^{3+}]^n + K_D^n}$$

where K_D represents the apparent microscopic dissociation constant and n is the Hill coefficient, indicating the maximum number of binding sites. All data were elaborated using the OriginPro 2018 software. Reverse titration experiments were performed by treating a solution of $FeCl_3$ at a concentration of 60 μM in MeOH with increasing peptide concentrations, ranging from 0.5 μM to 100 μM.[44]

CD measurements. CD spectra were recorded at room temperature using a Jasco J-810 spectropolarimeter using the quartz cell of 0.1 cm and 1 cm of path length for the far UV and near UV-visible regions, respectively. Data were collected with 1 nm bandwidth and 200 nm min^{-1} scanning speed. The variations in the α-helix structure upon Fe^{3+} addition were achieved by dissolving the peptide in MeOH at a concentration of 75 μM in a cell of 0.1 cm, and various volumes of a fresh solution of $FeCl_3$ were added to achieve Fe^{3+} to peptide ratios of 0.1, 0.3 and 0.6. All CD spectra were recorded in the 200–260 nm spectral range.

Cotton effects in the near UV-visible region from 350 nm to 700 nm were evaluated by dissolving the peptide in MeOH at a concentration of 100 μM and Fe^{3+} was added at the metal/peptide ratios of 0.1, 0.3 and 0.6.

ESI-MS measurements. Complexes with Fe^{3+} were prepared by dissolving pure peptides into MeOH at 1 mg mL^{-1} (~5 × 10^{-4} M) concentration.[45] 0.5 eq. of Fe^{3+} were added to the peptides, using a stock solution of 10 mM $FeCl_3$ in methanol. The solutions rapidly turned red/pink upon $FeCl_3$ addition. The solutions of the complexes (10 μL) were subjected to ESI-MS analysis using a Shimadzu LC-MS-2010EV system with an ESI interface, a Q-array-octapole-quadrupole mass analyzer, and the Shimadzu LC-MS solution Workstation software for data processing. All analyses were performed in a positive ion mode and a linear scan of m/z was performed in the following ranges: 800–1400; 1400–2000; 600–1200; and 1200–1800.[46] The samples were directly injected into the ESI source through a linear flow of acetonitrile 0.1% TFA at 0.5 mL min^{-1}.

FT-IR spectroscopy. The Fe^{3+} complexes were analyzed by FT-IR spectroscopy. The FT-IR spectra were recorded with a Nicolet Continuμm XL (Thermo Scientific) microscope in the wavenumber region of 400–4000 cm^{-1} with a resolution of 4 cm^{-1}. The blank was recorded using air as the reference. The complexes were prepared by dissolving pure peptides into methanol at 1 mg mL^{-1} (~5×10^{-4} M) concentration and 0.5 eq. of Fe^{3+}. The powdered complex was obtained by mixing, evaporating and freeze-drying the sample.

NMR spectroscopy. NMR samples were prepared by dissolving **Pep-cyc3** in 600 μL of CD_3OH (99.8% D, Sigma Aldrich) for a final concentration of 0.6–0.8 mM. The analyses of the peptide in free form and in the presence of different amounts of metal ions were performed using a Bruker 700 MHz spectrometer equipped with a *z*-gradient 5 mm triple-resonance cryoprobe. All measurements were made at 298 K. The spectra were calibrated relative to TSP (0.00 ppm) as an internal standard. The 2D TOCSY and NOESY spectra were recorded in the phase-sensitive mode using the method from States, using 4096 data points in *t*2 and 512 equidistant *t*1 values. The residual water signal was suppressed by the use of gradients. To exploit the metal binding properties of the peptide, increasing volumes (μL) of a stock solution of 29 mM of $ZnCl_2$ in CD_3OH were added to the peptide NMR tube. 1D proton spectra were obtained at Zn^{2+}/**Pep-cyc3** ratios of 0.05, 0.1, 0.15, 0.20, 0.25, 0.30, and 0.60. At *R* values equal to 0.2, 0.3, and 0.6, TOCSY and NOESY spectra were also acquired. One-dimensional spectra were processed and analysed using the MESTRENOVA 6.0 software (Mestrelab Research, S.L, Santiago de Compostela, Spain).

***In vitro* antibacterial activity of hydroxamate-based peptides.** The ability of hydroxamate-based peptides to chelate Fe^{3+} *in vitro* was investigated in the presence of iron-supplemented MHII agar (MHII + Fe^{3+}). The Mueller–Hinton No. 2 broth (MHII broth; cation adjusted) was purchased from Sigma-Aldrich (Milano, Italy). Iron-supplemented MHII agar (MHII + Fe^{3+}) was prepared as described elsewhere.[47] In particular, 0.5 mL of a freshly prepared 1 mg mL^{-1} filter-sterilized aqueous solution of $FeCl_3$ was added to 34 mL of melted MHII agar with gentle mixing. Then, the minimum inhibitory concentrations (MICs) were determined with a broth microdilution method according to the Clinical and Laboratory Standards Institute (CLSI) using 96-well microtiter plates.[48] In each well, 100 μL of fresh medium and 100 μL of microbial suspension were added, reaching a final concentration of 1×10^5 CFU mL^{-1}.[49] Peptides were used at concentrations ranging from 3.12 to 25 μM. After 24 h of incubation at 37 °C, the absorbance was measured at 590 nm wavelength by the turbidity method using an ELISA plate reader (SINERGY Ha BioTek).

Results and discussion

Grafting of iron chelators on the peptide Pep-cyc

During a bacterial infection, many Gram-negative pathogens synthesize small iron-sequestering molecules called siderophores as ferric iron is a key element for their colonization and replication.[50] Siderophores are classified according to the functional group chelating Fe^{3+} and the most abundant families are catecholate, hydroxamate, and carboxylate. Among these, the carboxylate siderophores have a lower affinity towards Fe^{3+} at physiological pH compared to the catecholate and hydroxamate groups.[51–53] Herein, we covalently bind hydroxamic acid as an iron-chelating siderophore at the C-terminal region of the cyclic peptide **Pep-cyc** to scavenge Fe^{3+} and induce the inhibition of the growth and replication of some Gram-negative pathogens. The peptide **Pep-cyc**, derived from a previous study performed on a temporin L analogue, is featured by a lactam bridge at positions 6 and 10 and assumes an amphipathic α-helix structure along residues Phe^5–Leu^{13}.[33] The free N-terminus, which is random in aqueous solution is important for the interaction with the membrane bilayer and thus for the activity. Therefore, the conjugation of the hydroxamate unit was performed in its helical C-terminal region and linkers of different lengths were used to warrant the exposure of the chelator. In particular, we used linkers of 7, 12 and 16 atoms yielding **Pep-cyc1**, **Pep-cyc2**, and **Pep-cyc3**, respectively (Fig. 2).

Hydroxamate-based cyclic peptides were assembled on the solid phase by using 2-chlorotrityl-*N*-Fmoc-hydroxylamine polymer-bound resin as the solid support to yield the C-terminal hydroxamic acid. Fmoc-Ahx-OH, Fmoc-GABA-OH, and Fmoc-PEG2-OH were chosen and introduced at C-terminus to have different linkers bearing the hydroxamate chelator after the peptide release from the resin. Before the peptide release, the lactam bridge was obtained on the resin by performing the palladium-catalyzed reaction between the residue Lys(Alloc) and Glu(OAll) at positions 6 and 10, respectively.

Binding of Fe^{3+} to hydroxamate-based peptides

The binding of Fe^{3+} to hydroxamate-based peptides designed in this study was investigated by UV-vis absorption spectroscopy. First, the UV-vis spectra of the peptides alone and $FeCl_3$ were acquired and compared to those of the complexes, prepared using a [Fe^{3+}]/[ligand] ratio of 0.22 (Fig. 3). The spectrum of $FeCl_3$ in the absence of peptides shows an absorption maximum at 360 nm, while all the Fe^{3+}–peptide complexes show a weak and broad absorption band between 450 and

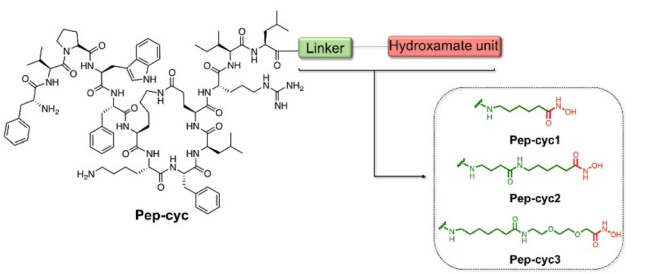

Fig. 2 Sequences of the designed peptides **Pep-cyc1**, **Pep-cyc2**, and **Pep-cyc3** featuring three different linkers bearing the hydroxamate unit.

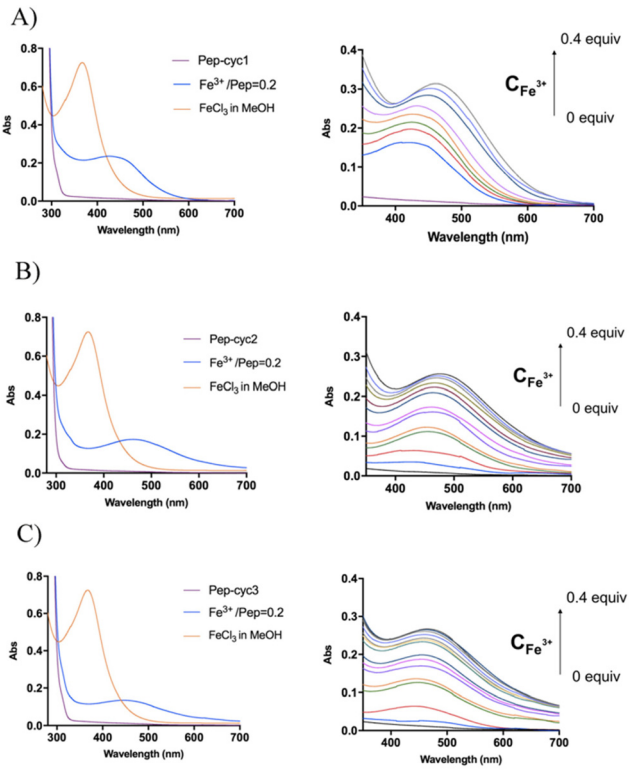

Fig. 3 UV spectra recorded for peptides **Pep-cyc1** (A), **Pep-cyc2** (B) and **Pep-cyc3** (C). On the left, the superimposition of the UV-vis spectra of peptide (purple trace), Fe^{3+} (orange trace) and the Fe^{3+}/ligand complex in the ratio of 0.2 (blue trace). On the right, UV-vis spectra acquired during the titration of the peptides with Fe^{3+} (0 to 0.4 eq.).

550 nm. The latter was assigned to a ligand-to-metal charge transfer (LMCT) transition in the Fe^{3+}–hydroxamate complexes.[54] Slight differences in the spectra were observed among the three peptides, which are likely to be related to the length of the linker, which may cause a different metal environment, thus modulating the complex interaction between the hydroxamate group and the metal ion. Complex formation was then monitored at 580 nm, where the contribution of absorption by unbound ferric ions is negligible. The spectrum of peptide **Pep-cyc**, lacking the hydroxamate group, was also acquired under the same experimental conditions. The latter did not show any absorption in this spectral range, providing preliminary evidence that no other functional group in the peptides is able to bind iron (see ESI, Fig. S4†).

Metal binding experiments were performed by titrating a solution containing a fixed ligand concentration (300 μM) with increasing amounts of Fe^{3+} in the range of 0–200 μM for **Pep-cyc2** and **Pep-cyc3** and of 0–500 μM for **Pep-cyc1**. As expected, the spectra showed a gradual increase in the absorbance at 480 nm for all the hydroxamate-based peptides, indicating the formation of iron complexes. For **Pep-cyc2** and **Pep-cyc3**, no significant change in the absorbance was observed at $[Fe^{3+}] >$ 120 μM, indicating binding saturation. Instead, in the case of **Pep-cyc1**, $[Fe^{3+}] >$ 300 μM was necessary to achieve saturation. The stoichiometry of the complexes was first evaluated by plotting the fraction of iron-bound peptide (α) as a function of Fe^{3+} concentration and applying separate linear regression to the unsaturated and saturated regions of the data points (Fig. 4, panel A). The point of intersection between the linear fit of the two datasets occurred at $[Fe^{3+}]$ of 104 and 93 μM for **Pep-cyc2** and **Pep-cyc3**, respectively, indicating the formation of FeL_3 complexes, as expected for the bidentate hydroxamate ligands (Fig. 5, panel A). In the case of **Pep-cyc1**, the intersection was found at 275 μM $[Fe^{3+}]$, suggesting the formation of a 1 : 1 Fe^{3+}–ligand complex (Fig. 5, panel B).

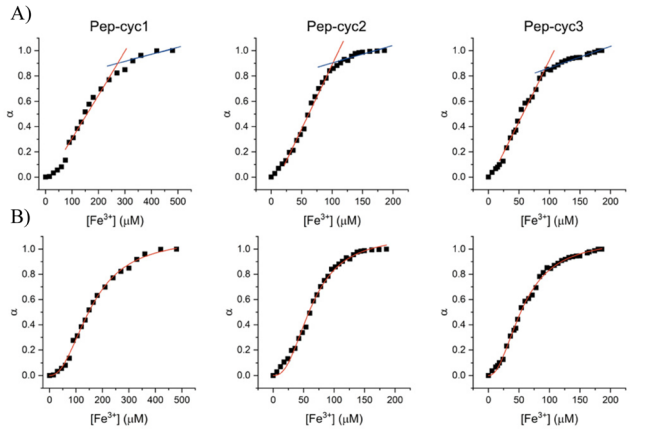

Fig. 4 Linear regression (panel A) and Hill (panel B) analyses of the fraction of bound peptide (α) as a function of $[Fe^{3+}]$.

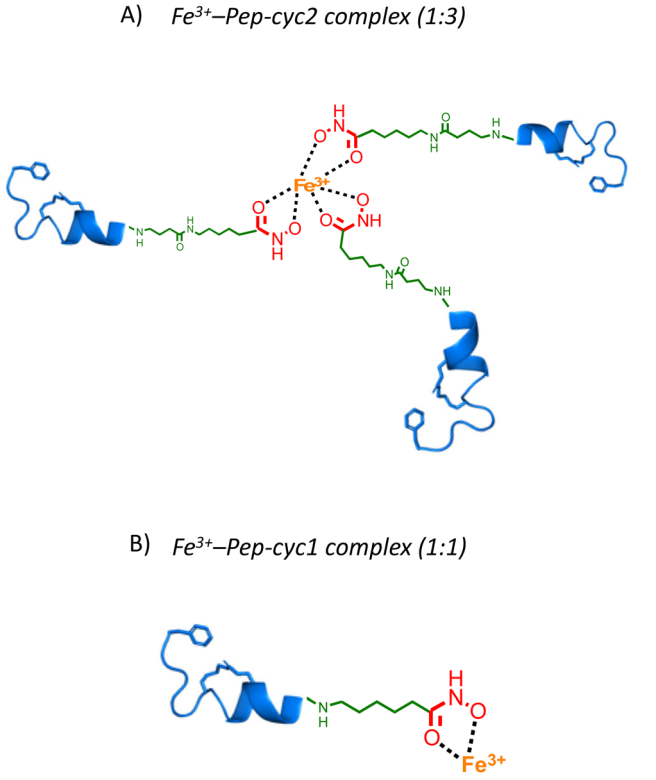

Fig. 5 Cartoon representing the coordination model structures of 1 : 1 Fe^{3+}–**Pep-cyc1** and 1 : 3 Fe^{3+}–**Pep-cyc2** complexes.

This finding could be explained by considering that **Pep-cyc1** contains the shortest linker to the hydroxamate group. Hence, the formation of the tris-chelate complex could be disfavored by steric interactions between the peptide ligands. The plot of α *vs.* [Fe^{3+}] showed a slow increase in low Fe^{3+} concentration, followed by a fast increase before reaching saturation. Such a behavior suggests that complex formation occurs in a stepwise process, rather than in a two-state equilibrium. Hill analysis of the experimental data allowed us to obtain the apparent dissociation constants (K_D) for the ferric complexes of all the hydroxamate-based peptides, which are 160 μM, 63 μM and 57 μM for **Pep-cyc1**, **Pep-cyc2** and **Pep-cyc3**, respectively (Fig. 4, panel B). A Hill coefficient of $n \approx 2$ was found in all cases, thus suggesting the presence of two different coordination sites in the iron complexes. Our hypothesis is that a cooperative effect would occur between the two donor oxygen atoms of the hydroxamate group, where the coordination of the carbonyl oxygen facilitates the deprotonation and, consequently, the binding of the carboxylate oxygen atom.

To further investigate the process of complex formation, reverse titration experiments were performed by treating a solution at a fixed Fe^{3+} concentration (60 μM) with increasing amounts of each peptide, ranging from 0.5 μM to 100 μM. The spectra obtained for **Pep-cyc1** (Fig. 6, panel A) revealed the appearance of an absorption maximum at 316 nm, concurrent to the decrease in the band at 380 nm, corresponding to unbound ferric ions. An additional broad absorption band centered at 490 nm appeared upon increasing the peptide concentration, resembling that observed by adding iron to an excess of ligand (Fig. 3).

The lack of isosbestic points between 360 and 490 nm indicates that multiple species are present in the solution at comparable concentrations of Fe^{3+} and peptide.

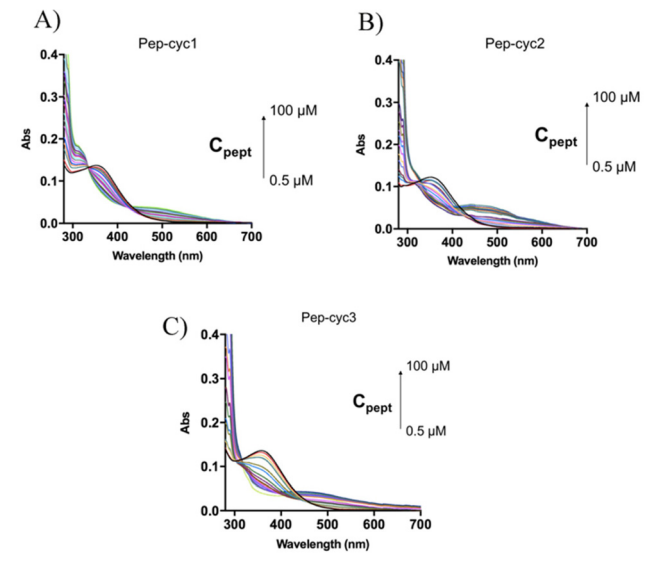

Fig. 6 UV-vis spectra acquired during the titration of Fe^{3+} (black line) with increasing peptide concentrations ranging from 0.5 μM to 100 μM: (A) **Pep-cyc1**; (B) **Pep-cyc2**; (C) **Pep-cyc3**.

In the cases of **Pep-cyc2** and **Pep-cyc3**, featuring the linker of intermediate and maximum lengths, respectively, the absorption band at 316 nm was not observed, while the broad absorption feature between 450 and 550 nm was still formed by increasing the peptide concentration (Fig. 6, panels B and C). The absence of isosbestic points further confirms the presence of multiple equilibria in the solution. These experiments were also performed on **Pep-cyc** and its linear analogue [Pro^3, $DLeu^9$]TL, displaying no complex formation (ESI Fig. S5†).

ESI-MS analysis of the Fe^{3+}–peptide complexes

The formation of the Fe^{3+} complexes of hydroxamate-based peptides was also investigated by ESI-MS analysis. Table 1 shows the most abundant ions found in the mass spectrum of each sample. Complexes with a 1 : 1 and 1 : 2 metal : ligand stoichiometry were observed for all peptides, while the FeL_3 complexes could not be detected in the experimental conditions of MS analysis.

FT-IR spectra analysis

The FTIR measurements were performed to identify the main functional groups of peptides involved in Fe^{3+} coordination. The transmittance band ranging from 4000 cm^{-1} to 400 cm^{-1} was recorded for the FTIR spectra as depicted in Fig. 7. In particular, the spectra collected for the peptide **Pep-cyc** showed no difference compared to the spectra recorded in the presence and in the absence of Fe^{3+}, indicating that there are no interactions between **Pep-cyc** and Fe^{3+}, in accordance with the other experimental data. The FTIR spectra collected for the peptide **Pep-cyc3** in the presence and in the absence of Fe^{3+} showed significant differences. The –OH (alcohol) that arises at 2933 in **Pep-cyc3** is shifted to 2927 cm^{-1} following the Fe^{3+} coordination. Furthermore, the frequency of C=O at 1178 cm^{-1} is shifted to 1192 and almost disappears after the Fe^{3+} coordination. All these data support iron coordination with hydroxamic acid.[55]

Circular dichroism (CD) spectroscopy

The peptide **Pep-cyc** adopts an α-helix structure along the residues 5–13 in the presence of micelles mimicking the bacterial membrane. We evaluated the effect of the metal binding on the secondary structure by using CD spectroscopy (Fig. 8).[56]

Table 1 The most abundant ions found by ESI-MS

Ion	Calculated mass	Experimental mass
[**Pep-cyc1** + $2H^+$]$^{2+}$	917.64	918.00
[**Pep-cyc1** − H^+ + Fe^{3+}]$^{2+}$	944.05	944.75
[**2Pep-cyc1** − H^+ + Fe^{3+}]$^{2+}$	1861.1	1860.35
[**Pep-cyc2** + $2H^+$]$^{2+}$	960.69	960.20
[**Pep-cyc2** − H^+ + Fe^{3+}]$^{2+}$	986.54	986.85
[**2Pep-cyc2** + Fe^{3+} + H^+ + H_2O]$^{4+}$	978.99	978.40
[**Pep-cyc3** + $2H^+$]$^{2+}$	989.72	990.35
[**Pep-cyc3** − H^+ + Fe^{3+}]$^{2+}$	1016.72	1017.05
[**2Pep-cyc3** + Fe^{3+}]$^{3+}$	1336.33	1337.85

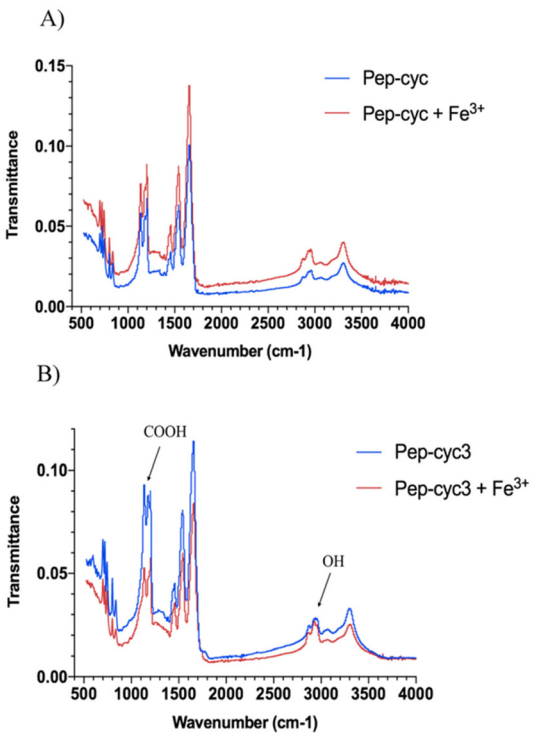

Fig. 7 IR spectra of peptides **Pep-cyc** (panel A) and **Pep-cyc3** (panel B) alone and their complexes with Fe^{3+}.

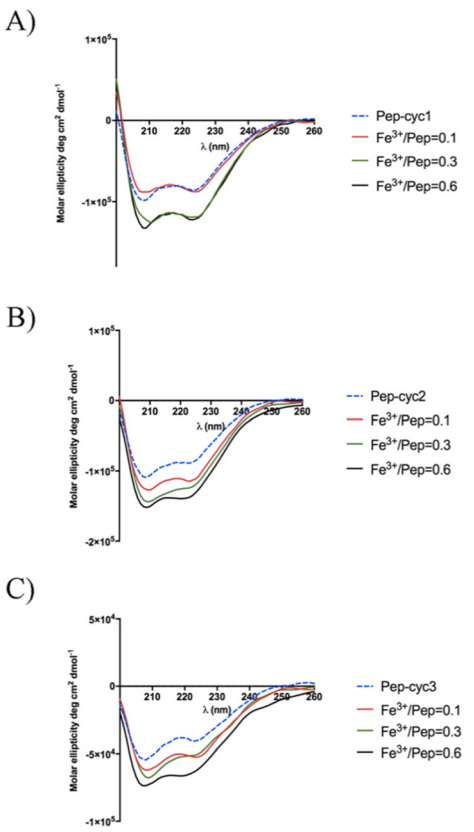

Fig. 8 CD spectra of the titration of peptides with Fe^{3+} in the Fe^{3+}/peptide ratios of 0.1, 0.3 and 0.6.

Each peptide alone in MeOH adopts an α-helix conformation as the peptide **Pep-cyc** without iron chelator. The helical content for each peptide increases upon increasing Fe^{3+} concentrations, as evidenced by Fig. 8. Regardless of the linker length, a significant increase in the helical content was observed at the Fe^{3+}/peptide ratio of 0.3 for each peptide as detected by CD spectra.

CD spectroscopy was also used to explore the Cotton effect of the Fe^{3+}–peptide complexes in the near UV and visible regions. Inspection of the CD spectra in the range 300–400 nm showed the absence of any peak (data not shown) suggesting the presence of a racemic mixture of the two enantiomeric forms lambda (Λ) and delta (Δ) that are typical of metal tris chelates.

NMR spectroscopy

Among the peptides, **Pep-cyc3** with the longest linker-bearing hydroxamate unit was analysed also by NMR. The measurements were performed in MeOH, the best solvent system among those tested. The analysis allowed us to verify the structure of the construct. The observation of the NOE effect between the δNH proton of Q^{10} and the εε′ protons of K^6 confirms the condensation between the residue side chains and thus the cyclization of the [K^6KFlQ^{10}] segment. The linking to the C-terminal residue L^{13} of the tail formed by Ahx and PEG2 was verified by the presence of signals which, in terms of pattern and chemical shift values, correspond to those expected for them. The assignment of the terminal hydroxamate moiety, complicated by the unobservability of the NH-OH protons due to the chemical exchange phenomena (and tautomerism), was based on the presence of a singlet at 4.03 ppm consistent with the chemical shift expected for the hydroxamate adjacent CH_2 protons. The line width and the scarcity of the NOE effects hindered the definition of the conformational organization of the peptide while suggesting aggregation phenomena at the concentrations used. Once confirmed that the structure of **Pep-cyc3** corresponds to the design one, the aim of the investigation was also to test the binding properties of the system towards metal ions. In the first phase of the study, it was decided to evaluate the response of the peptide to the diamagnetic Zn^{2+} ion. The 1D and 2D spectra of the peptide were acquired in the presence of increasing amounts of Zn^{2+}, up to a Zn^{2+}/**Pep-cyc3** ratio equal to 0.6 (Fig. 9). The spectral changes produced by the addition of metal ion are observable in Fig. 8. The mainly affected signals are those of the amide proton αNH of F^8 (8.23 ppm), εNH of K^6 (7.84 ppm), NH of PEG2 (8.09 ppm), 6-NH (7.56 ppm) of the amino-hexanoic acid segment, CH_2 adjacent to the hydroxamate moiety (4.03 ppm), and δδ′ CH_2 of K^6 (2.71 ppm).

The sensitivity of proton signals belonging to the C-terminal tail and the cycle [K^6KFlQ^{10}] to metal addition suggests that both the tail and the cycle may be sites of metal coordination. The identification of the tail site agrees with the results obtained through other techniques. The

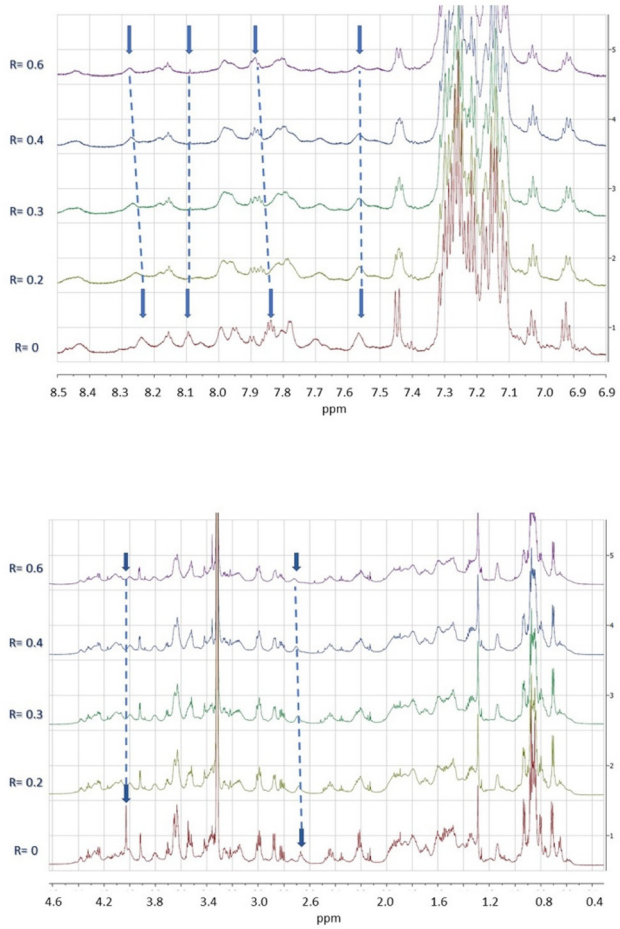

Fig. 9 Superimposition of low field (up) and high field regions (down) of the 1H NMR spectra of **Pep-cyc3** at different values of Zn^{2+}/peptide ratios (*R*). Signals most sensible to metal ion addition are indicated by blue arrows.

possibility that the cyclic structure could also function as a ligand is only observed by NMR. This is in line with the higher peptide concentration needed for this technique compared to that useful for the others, and possibly with the use of Zn^{2+} as an ersatz ion for the target paramagnetic Fe^{3+}. However, it is interesting to note that since the addition of zinc ions to the peptide solution does not perturb all signals of the proton spectra to the same degree, thus indicating the occurrence of a region-specific interaction. The signals most affected by metal ions are those belonging to the most interacting peptide surfaces. We found that the diamagnetic analyses reported here confirm the binding properties of **Pep-cyc3** and successfully localize the major metal ion binding site. The NMR data of **Pep-cyc3** with Zn(II) diamagnetic ions have surprisingly shown that the adduct may room two coordination sites. This is a relevant piece of information for efficiently planning the NMR work with the paramagnetic **Pep-cyc3**/Fe(III) system.

Hydroxamate-based peptides inhibit bacterial growth

The metal binding of hydroxamate-based peptides was evaluated *in vitro* by determining the minimum inhibitory concentration (MIC) in the presence of iron-supplemented MHII agar (MHII + Fe^{3+}) and in the absence of Fe^{3+} (MHII − Fe^{3+}). In this study, the inhibition of the bacterial growth of two Gram-negative strains, *E. coli* ATCC 25922 and *K. pneumoniae* ATCC 13883, was evaluated (Table 2).

The MIC values of peptide **Pep-cyc** were the same in the presence and in the absence of ferric iron confirming that the peptide did not chelate the metal. The conjugation of the hydroxamate chelating unit did not induce a significant modification in the activity of the native peptides as shown by the results obtained in the presence of MHII − Fe^{3+}, characterized by the absence of iron. The MIC values against *K. pneumoniae* became remarkably lower in MHII + Fe^{3+}, especially for the peptide **Pep-cyc3** bearing the longest linker. In fact, **Pep-cyc3** had a high MIC value of 25 μM in the absence of the metal, while a significant decrease in its MIC value (6.25 μM) was calculated in MHII + Fe^{3+} attributed to its strong affinity and ability to chelate Fe^{3+}. Moreover, a reduction in the MIC value (3.12 μM) on *K. pneumoniae* was also observed for the peptide **Pep-cyc2** featured by a linker of intermediate length and ability to chelate Fe^{3+} with the formation of a FeL_3 complex as showed in UV measurements. Regarding the peptide **Pep-cyc1** bearing the shortest linker and endowed with a lower capacity to chelate the metal (as shown by the K_D), there was also a significant activity with a MIC of 3.12 μM in the presence of metal, indicating that the amount of iron subtracted from the bacteria is sufficient to induce an increase in activity.

However, we also observed a reduction in the MIC values of *E. coli* for all peptides in the presence of MHII + Fe^{3+}, but they were less significant than those obtained for *K. pneumoniae*.

Overall, the reduction in the MIC values of hydroxamate-based peptides both on *K. pneumoniae* and *E. coli* is clearly due to their coordination of Fe^{3+} that negatively influences bacterial growth through the sequestration of available ferric iron away from bacteria.

Table 2 MIC values (μM) of peptides under varying concentrations of Fe^{3+}

	Pep-cyc		**Pep-cyc1**		**Pep-cyc2**		**Pep-cyc3**	
Bacteria	MHII − Fe^{3+}	MHII + Fe^{3+}	MHII − Fe^{3+}	MHII + Fe^{3+}	MHII − Fe^{3+}	MHII + Fe^{3+}	MHII − Fe^{3+}	MHII + Fe^{3+}
E. coli ATCC 25922	25	>25	>25	12.5	>25	12.5	>25	25
K. pneumoniae ATCC 13883	12.5	12.5	12.5	3.12	12.5	3.12	25	6.25

Conclusions

Siderophore conjugation to antibacterial molecules represents a challenging research area to generate new molecules to treat Gram-negative infections. The presence of LPS in their outer membranes acts as a complex barrier against the penetration and diffusion of antibiotics into Gram-negative bacterial cells, making the development of new antibiotics more challenging. This work describes the effectiveness to conjugate small iron-chelator units to enhance the antimicrobial activity of AMPs against some Gram-negative pathogens. Here, we designed and synthesized three cyclic peptides **Pep-cyc1**, **Pep-cyc2**, and **Pep-cyc3** by introducing in their C-terminus the hydroxamate siderophore bound to three linkers of lengths 7, 12, and 16 atoms, respectively.

The UV-vis titration of each peptide with a solution of Fe^{3+} evidenced the presence of weak and broad absorption band complexes. By plotting the fraction of iron-bound peptide as a function of Fe^{3+} concentration, we observed that the complex formation occurs in a stepwise process. Moreover, we determined the formation of FeL_3 complexes for the peptides **Pep-cyc2** and **Pep-cyc3** endowed with longer linkers, while we observed the formation of a 1 : 1 Fe^{3+}–peptide for **Pep-cyc1** with the shortest linker. Through the Hill equation, we also calculated K_D values for the Fe^{3+}–**Pep-cyc2** and Fe^{3+}–**Pep-cyc3** complexes of 63 μM and 57 μM, respectively, while a higher K_D of 160 μM was obtained for the Fe^{3+}–**Pep-cyc1** complex. Furthermore, we obtained a Hill coefficient of 2 for all the peptides suggesting a cooperative effect that could occur between two donor oxygen atoms of the hydroxamate group during the complex formation, where we supposed that the coordination of the carbonyl oxygen facilitates the deprotonation and, consequently, the binding of the carboxylate oxygen atom. The coordination of the hydroxamate unit was further confirmed by FTIR, where the frequency of the carbonyl group at 1178 cm^{-1} is shifted at 1192, while the signal of the hydroxyl group is shifted from 2933 to 2927 cm^{-1}. In addition, in the CD spectra recorded in the visible region, no Cotton effect was observed during the complex formation and we hypothesized the formation of a racemic mixture of the enantiomeric forms Λ and Δ.

Our UV-vis and NMR data strongly support the antimicrobial results obtained *in vitro* on some Gram-negative strains, demonstrating the key role played by the efficacious metal coordination of all our hydroxamate-based peptides. In particular, in the presence of MHII + Fe^{3+}, peptides **Pep-cyc2** and **Pep-cyc3** having better affinity towards Fe^{3+} caused the inhibition of the growth of *K. pneumoniae* and *E. coli* with MIC values ranging from 6.25 to 3.12 μM in comparison with those obtained in the absence of Fe^{3+}.

In conclusion, siderophore conjugation may represent a valid opportunity for improving the activity and selectivity of some AMPs used for the treatment of infectious diseases caused especially by Gram-negative pathogens, acting as potential molecules to add to our current antibiotic arsenal.

Author contributions

The manuscript was written through the contributions of all authors. All authors approved the final version of the manuscript.

Conflicts of interest

There are no conflicts to declare.

Acknowledgements

Rosa Bellavita (R. B.) was supported by Fondazione Umberto Veronesi. R. B. thanks the Department of Pharmacy for supporting this work in the frame of the Department of Excellence. This work was partly supported by MISE-Contratto di Sviluppo (CdS) "Altergon Italia" project 000463. This research was funded by FRA (Finanziamento della Ricerca di Ateneo (FRA) linea B_2021), University of Naples, "Federico II".

References

1 E. R. Frawley and F. C. Fang, *Mol. Microbiol.*, 2014, **93**, 609–616.
2 V. Braun and K. Hantke, *Curr. Opin. Chem. Biol.*, 2011, **15**, 328–334.
3 T. Goswami, A. Rolfs and M. A. Hediger, *Biochem. Cell Biol.*, 2002, **80**, 679–689.
4 P. L. Carver, *Curr. Med. Chem.*, 2018, **25**, 85–96.
5 K. N. Raymond, B. E. Allred and A. K. Sia, *Acc. Chem. Res.*, 2015, **48**, 2496–2505.
6 T. Zheng and E. M. Nolan, *Metallomics*, 2012, **4**, 866–880.
7 B. C. Chu, A. Garcia-Herrero, T. H. Johanson, K. D. Krewulak, C. K. Lau, R. S. Peacock, Z. Slavinskaya and H. J. Vogel, *Biometals*, 2010, **23**, 601–611.
8 J. Kramer, Ö. Özkaya and R. Kümmerli, *Nat. Rev. Microbiol.*, 2020, **18**, 152–163.
9 R. C. Hider and X. Kong, *Nat. Prod. Rep.*, 2010, **27**, 637–657.
10 M. Miethke and M. A. Marahiel, *Microbiol. Mol. Biol. Rev.*, 2007, **71**, 413–451.
11 I. J. Schalk, M. Hannauer and A. Braud, *Environ. Microbiol.*, 2011, **13**, 2844–2854.
12 M. X. Zhang, C. F. Zhu, Y. J. Zhou, X. L. Kong, R. C. Hider and T. Zhou, *Chem. Biol. Drug Des.*, 2014, **84**, 659–668.
13 M. G. P. Page, *Clin. Infect. Dis.*, 2019, **69**, S529–S537.
14 R. C. Hider and X. Kong, *Nat. Prod. Rep.*, 2010, **27**, 637–657.
15 G. Centola, F. Xue and A. Wilks, *Metallomics*, 2020, **12**, 1863–1877.
16 S. A. Cotton, *J. Coord. Chem.*, 2018, **71**, 3415–3443.
17 H. Boukhalfa, S. D. Reilly, R. Michalczyk, S. Iyer and M. P. Neu, *Inorg. Chem.*, 2006, **45**, 5607–5616.
18 T. Palanché, S. Blanc, C. Hennard, M. A. Abdallah and A. M. Albrecht-Gary, *Inorg. Chem.*, 2004, **43**, 1137–1152.

19 K. H. Negash, J. K. S. Norris and J. T. Hodgkinson, *Molecules*, 2019, **24**, 3314.
20 A. C. Gomes, A. C. Moreira, G. Mesquita and M. S. Gomes, *Pharmaceuticals*, 2018, **11**, 84.
21 S. Zhao, Z. P. Wang, X. Wen, S. Li, G. Wei, J. Guo and Y. He, *Org. Lett.*, 2020, **22**, 6632–6636.
22 R. Zhang, L. Xu and C. Dong, *Protein Pept. Lett.*, 2022, **29**, 641–650.
23 V. Del Genio, A. Falanga, E. Allard-Vannier, K. Hervé-Aubert, M. Leone, R. Bellavita, R. Uzbekov, I. Chourpa and S. Galdiero, *Pharmaceutics*, 2022, **14**, 1235.
24 C. Zhang and M. Yang, *Antibiotics*, 2022, **11**, 349.
25 J. Talapko, T. Meštrović, M. Juzbašić, M. Tomas, S. Erić, L. Horvat Aleksijević, S. Bekić, D. Schwarz, S. Matić, M. Neuberg and I. Škrlec, *Antibiotics*, 2022, **11**, 1417.
26 A. Maione, R. Bellavita, E. de Alteriis, S. Galdiero, L. Albarano, A. La Pietra, M. Guida, E. Parrilli, C. D'Angelo, E. Galdiero and A. Falanga, *Int. J. Mol. Sci.*, 2022, **23**, 2151.
27 A. Falanga, A. Maione, A. La Pietra, E. de Alteriis, S. Vitale, R. Bellavita, R. Carotenuto, D. Turrà, S. Galdiero, E. Galdiero and M. Guida, *Pharmaceutics*, 2022, **14**, 1167.
28 R. Oliva, M. Chino, K. Pane, V. Pistorio, A. De Santis, E. Pizzo, G. D'Errico, V. Pavone, A. Lombardi, P. Del Vecchio, E. Notomista, F. Nastri and L. Petraccone, *Sci. Rep.*, 2018, **8**, 8888.
29 K. A. Parsels, K. A. Mastro, J. M. Steele, S. J. Thomas and W. D. Kufel, *J. Antimicrob. Chemother.*, 2021, **76**, 1379–1391.
30 J. H. Boyce, B. Dang, B. Ary, Q. Edmondson, C. S. Craik, W. F. DeGrado and I. B. Seiple, *J. Am. Chem. Soc.*, 2020, **142**, 21310–21321.
31 D. Y. Kim and H. J. Kim, *Org. Lett.*, 2021, **23**, 5256–5260.
32 J. Oh, D. Kang, S. Hong, S. H. Kim, J. H. Choi and J. Seo, *Dalton Trans.*, 2021, **50**, 3459.
33 R. Bellavita, B. Casciaro, S. Di Maro, D. Brancaccio, A. Carotenuto, A. Falanga, F. Cappiello, E. Buommino, S. Galdiero, E. Novellino, T. N. Grossmann, M. L. Mangoni, F. Merlino and P. Grieco, *J. Med. Chem.*, 2021, **64**, 11675–11694.
34 M. L. Mangoni, *Cell. Mol. Life Sci.*, 2006, **63**, 1060–1069.
35 S. M. Romero, A. B. Cardillo, M. C. Martínez Ceron, S. A. Camperi and S. L. Giudicessi, *Surg. Infect.*, 2020, **21**, 309–322.
36 R. Bellavita, A. Vollaro, M. R. Catania, F. Merlino, L. De Martino, F. P. Nocera, M. DellaGreca, F. Lembo, P. Grieco and E. Buommino, *Antibiotics*, 2020, **9**, 530.
37 E. Roscetto, R. Bellavita, R. Paolillo, F. Merlino, N. Molfetta, P. Grieco, E. Buommino and M. R. Catania, *Antibiotics*, 2021, **10**, 1312.
38 C. Zannella, A. Chianese, L. Palomba, M. E. Marcocci, R. Bellavita, F. Merlino, P. Grieco, V. Folliero, A. De Filippis, M. L. Mangoni, L. Nencioni, G. Franci and M. Galdiero, *Int. J. Mol. Sci.*, 2022, **23**, 2060.
39 R. Bellavita, A. Falanga, F. Merlino, G. D'Auria, N. Molfetta, A. Saviano, F. Maione, U. Galdiero, M. R. Catania, S. Galdiero, P. Grieco, E. Roscetto, L. Falcigno and E. Buommino, *J. Enzyme Inhib. Med. Chem.*, 2023, **38**, 36–50.
40 R. Bellavita, A. Maione, F. Merlino, A. Siciliano, P. Dardano, L. De Stefano, S. Galdiero, E. Galdiero, P. Grieco and A. Falanga, *Pharmaceutics*, 2022, **14**, 454.
41 Y. Sixto-López, J. A. Gómez-Vidal, N. de Pedro, M. Bello, M. C. Rosales-Hernández and J. Correa-Basurto, *Sci. Rep.*, 2020, **10**, 10462.
42 A. M. Yousif, V. Ingangi, F. Merlino, D. Brancaccio, M. Minopoli, R. Bellavita, E. Novellino, M. V. Carriero, A. Carotenuto and P. Grieco, *Eur. J. Med. Chem.*, 2018, **143**, 348–360.
43 D. M. Al Shaer, F. Albericio and B. G. de la Torre, *ChemistrySelect*, 2021, **6**, 7674–7681.
44 Y. Yang, J. Liu, L. Yang, K. Li, H. Zhang, S. Luo and L. Rao, *Dalton Trans.*, 2015, **44**, 8959–8970.
45 G. De Tommaso, M. M. Salvatore, R. Nicoletti, M. DellaGreca, F. Vinale, A. Staropoli, F. Salvatore, M. Lorito, M. Iuliano and A. Andolfi, *Toxics*, 2021, **9**, 19.
46 E. Orlowska, A. Roller, H. Wiesinger, M. Pignitter, F. Jirsa, R. Krachler, W. Kandioller and B. K. Kepplera, *RSC Adv.*, 2016, **6**, 40238–40249.
47 T. A. Wencewicz, T. E. Long, U. Möllmann and M. J. Miller, *Bioconjugate Chem.*, 2013, **24**, 473–486.
48 CLSI, Methods for diluition antimicrobial susceptibility tests for bacteria that grow aerobically; approved standards-6, in *Document m7-a6 Performance Standards for Antimicrobial Susceptibility Testing*, CLSI, Wayne PA, USA, 2006.
49 E. de Alteriis, A. Maione, A. Falanga, R. Bellavita, S. Galdiero, L. Albarano, M. M. Salvatore, E. Galdiero and M. Guida, *Antibiotics*, 2021, **11**, 26.
50 A. Garénaux, M. Caza and C. M. Dozois, *Vet. Microbiol.*, 2011, **153**, 89–98.
51 C. J. Carrano, H. Drechsel, D. Kaiser, G. Jung, B. Matzanke, G. Winkelmann, N. Rochel and A. M. Albrecht-Gary, *Inorg. Chem.*, 1996, **35**, 6429–6436.
52 F. Garzón-Posse, Y. Quevedo-Acosta, C. Mahecha-Mahecha and P. Acosta-Guzmán, *Eur. J. Org. Chem.*, 2019, **48**, 7747–7769.
53 J. Keth, T. Johann and H. Frey, *Biomacromolecules*, 2020, **21**, 2546–2556.
54 T. Inomata, H. Eguchi, Y. Funahashi, T. Ozawa and H. Masuda, *Langmuir*, 2012, **28**, 1611–1617.
55 L. R. Hassan, E. H. Anouar, H. Bahron, F. Abdullah and A. Mohd Tajuddin, *J. Biol. Inorg. Chem.*, 2020, **25**, 239–252.
56 S. Futaki, T. Kiwada and Y. Sugiura, *J. Am. Chem. Soc.*, 2004, **126**, 15762–15769.